
This is an electronic reprint of the original article.
This reprint may differ from the original in pagination and typographic detail.

Olafsson, Dagur; Santos Vilaca da Silva, Pedro; Vesanko, Jussi
Characterization of FSW of Aluminium to Copper for Electrical Busbars

Published in:
71th Annual Assembly of International Institute of Welding (IIW2018)

Published: 15/07/2018

Document Version
Publisher's PDF, also known as Version of record

Please cite the original version:
Olafsson, D., Santos Vilaca da Silva, P., & Vesanko, J. (2018). Characterization of FSW of Aluminium to Copper for Electrical Busbars. In *71th Annual Assembly of International Institute of Welding (IIW2018): Commission III-B Article III-1859-18*

This material is protected by copyright and other intellectual property rights, and duplication or sale of all or part of any of the repository collections is not permitted, except that material may be duplicated by you for your research use or educational purposes in electronic or print form. You must obtain permission for any other use. Electronic or print copies may not be offered, whether for sale or otherwise to anyone who is not an authorised user.

Characterization of FSW of Aluminium to Copper for Electrical Busbars

Dagur Ólafsson¹, Pedro Vilaça^{1*}, Jussi Vesanko²

¹ *Department of Mechanical Engineering, School of Engineering, Aalto University, Finland*

² *Promeco Oy, Kankaanpää, Finland*

* *Corresponding author: pedro.vilaca@aalto.fi; +358 50 3652110*

Abstract

In this work it is investigated the metallurgical, mechanical and electrical properties of Aluminum-Copper (Al-Cu) butt joints made by Friction Stir Welding (FSW) to be applied as Al busbars with Cu ends. The application of Al busbars in electrical industry faces one major challenge in the joining to peripheral components typically made of Cu. The joining of Al to Cu is one major challenge, because there are not many feasible welding techniques able to overcome the different physical properties and deliver a sound structural joint. Thus, bolted joints are a common solution. To lower the inherent contact resistance of this solution high clamping forces are required, but while in operation, the dissimilar bolted joint undergoes fast relaxation of the force, demanding frequent maintenance. The base materials investigated are AA1050 H14/24 and Cu OF 04, with thickness of 6 mm. To understand the benefits of having an Al bus bar with Cu bolted end, compared with one made of monolithic Al material, a dedicated experimental test setup and protocol was designed and implemented. This experimental test enables to monitor the force relaxation of a pre-loaded bolt joint, under cyclic thermal loading, simulating real operational conditions. The test was applied to both Al base material and Cu base material components. The experimental results show that the force relaxation in the Cu bolted joint was about 50% lower compared with the Al. Thus, bus bars with Cu ends are more stable and will need less maintenance while in operation than bus bars with Al ends.

Optimized welding conditions were implemented and thoroughly characterized. Tensile, bending and microhardness tests were used to establish the mechanical properties. Optical microscope (OM) and scanning electron microscopy (SEM) were used to characterize the microstructure. Joining mechanisms and intermetallic compounds in the weld were investigated using energy dispersive x-ray spectroscopy (EDX). The electrical resistance of the weld was assessed using a microhmmeter. The properties of this optimized weld resulted in 85% Global Efficiency to Tensile Strength and 41% Global Efficiency to Bending compared to the Al base material, and 97% electrical conductivity efficiency compared to an ideal bimetallic component made of the same materials with no contact resistance. The resistance of the FSW joint is 200 times lower than the contact resistance between the base materials while under a high force.

Keywords (IIW Thesaurus): Friction Stir Welding, Aluminum, Copper, Busbars; Electrical Resistance, Intermetallic Compounds; Mechanical Properties.

1. Introduction

Various industries constantly strive to improve their competitiveness, with higher performance products made with efficient processes with low environmental impact. Most of the developments are supported by material optimization demanding advanced solution for processing, namely joining. The research and engineering community works towards meeting these demands, willing to transfer the innovative solutions and know-how into industry. Friction Stir Welding (FSW) is a solid-state material joining technology, which opens up possibilities in bimetallic joints of dissimilar materials that is almost impossible to do with conventional fusion welding methods. Welded joints such as aluminium (Al) to steel, Al to copper (Cu) and steels to other highly dissimilar iron based components have become a possibility as the process joins materials without melting them. This has opened up new possibilities in the design optimization and manufacturing of various products. E.g. in electrical applications enables to combine cheaper and lighter material, such as Al, with Cu that has low electrical resistance, with more stable properties and corrosion resistance in a wider temperature ranges.

Busbars are conductive strips or bars used for short distance high current power transference. In recent years, the material choice for busbars has been changing from Cu to Al due to the lower price of Al. The decrease in the direct cost of the busbar is attractive, but perhaps short-sighted. High clamping forces are required for busbar connections to minimize the contact resistance between the busbars and other components. These high forces, along with the temperature changes the connections experience while in operation, slowly deform the pressed material, which in turn lowers the clamping forces. To avoid component failure, the connection therefore needs to be retightened periodically. This results in maintenance costs, and increases the life cycle price of the Al busbar.

Temperature changes under high pressures affect materials differently. Elevated temperatures affect Al alloys commonly used for busbars such as EN-EW-6101-T4 more than high conductive Cu alloys like Cu-OF [1, 2]. The thermal expansion coefficient is also higher for Al than for Cu [3]. These differences between the two materials might explain the higher maintenance associated with Al busbars.

A potential solution to this problem is to use bimetallic busbars made from both materials, Al and Cu. A busbar mainly composed of Al but with Cu ends has the advantage of being cheaper and lighter than a monolithic Cu bus bar but avoids the increase in maintenance cost associated with monolithic Al busbars. For this solution to be viable, these bimetallic busbars need to be manufactured efficiently.

Invented in 1991 by Wayne Thomas and his colleagues at the welding institute in the United Kingdom [4], FSW welds by rotating a non-consumable tool inside the materials to be welded in order to soften them locally using heat generated by friction and plastic deformation. Once softened, the joint surfaces are stirred and joined, still in their solid state, as the materials do not reach their melting temperatures. This increases the weld quality compared to fusion welding as it avoids the many problems associated with fusion welding such as changes in volume, gas solubility, distortion and residual stress [5].

FSW has numerous other benefits unrelated to the quality of welds. It has been shown to nearly reduce the emission of hazardous fumes to zero as well as to reduce the energy used during welding, therefore having less environmental impact than other more traditional welding techniques. The process can be used in all orientations as gravity has negligible impact during FSW. Due to high forces the process is typically fully mechanized which increases the equipment cost while lowering the skill requirements and cost of operators [5].

As a solid-state process, FSW operates under the fusion temperatures of the materials it is joining. It has therefore opened up possibilities to weld dissimilar materials with very different properties that normally create problems for fusion welding. Difference in fusion temperatures, as with Cu and Al make it near to impossible to acquire sound welds with fusion welding. Several issues like different deformation behaviors, formation of Intermetallic Compounds (IMCs) and differences in physical properties promote asymmetry in the flow of material and heat during dissimilar FSW and need to be taken into account [6].

IMCs are defined as solid phases containing two or more metallic elements, with optionally one or more non-metallic elements, whose crystal structure differs from that of the other constituents [7]. They are generally very stable, brittle and with a high fusion temperature. They pose a problem in the welding of dissimilar materials, both in fusion and solid-state welding. In fusion welding they are generally formed during the solidification of the melted metals. In FSW, they form under high pressures and intense plastic deformation [8]. In fusion welding of dissimilar materials the amount of intermetallic compounds is so that it compromises the weld in almost every case and renders the welding method useless for many material combinations such as Al and Cu.

In this work, the difference in force relaxation rates between Cu-OF-04 and strain hardened EN-EW-6101-T4 under a 40 kN clamping force from a bolt while under cyclic thermal loading, simulating a busbar connection while in operation, is investigated. A 6 mm AA1050-H14/24 – Cu-OF-04 FSW joint, optimized with busbar production in mind, was thoroughly characterized. Tensile, bending and microhardness tests were used to establish the mechanical properties. Optical microscope and scanning electron microscope were used to investigate the microstructure. Joining mechanisms and intermetallic compounds in the weld were investigated using an X-ray diffraction analysis. The electrical resistance of the weld was assessed using a microhmmer.

2. Experimental procedure

Clamping force relaxation experiment

The experimental set up, presented in Fig. 1, is made of several parts. A strain-gauge load cell and the bus bar end are clamped together between a bolt and a nut, separated by stainless steel washers and a load pyramid, which transfers the load from the larger load cell to the small end of the bus bar. Behind the flattened mounting end of the bus bar, cartridge heaters are placed and a cooling channel is made. To monitor the thermal cycles, three k-type thermocouple wires are welded to the sides of the clamped area of the bus bar using electron discharge welding.

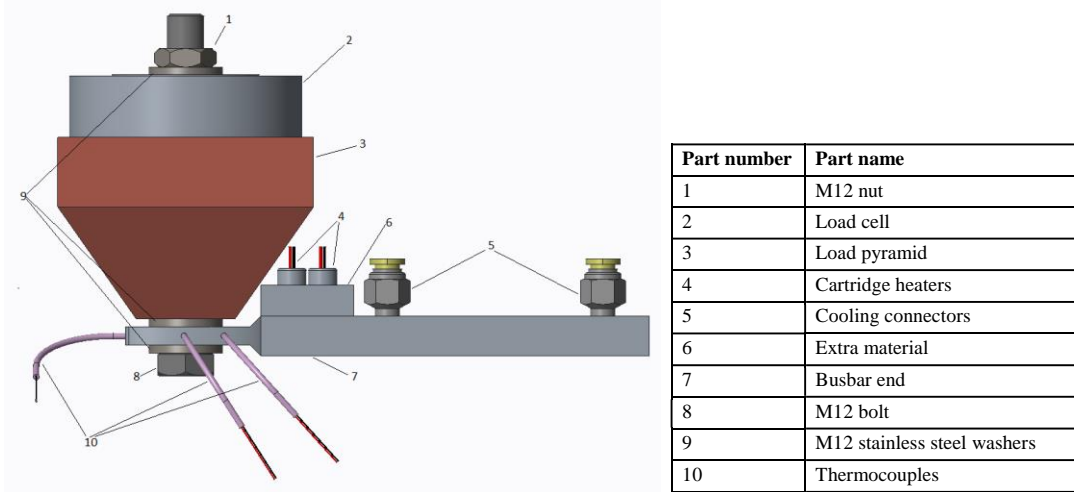


Fig. 1 Experimental set up of the clamping force relaxation experiment

The test was controlled by a microcontroller and conducted as follows: The force and temperature monitoring is activated and the data is sampled and logged with certain sampling frequencies, f_F and f_T . The bolt is preloaded with a certain force, F_0 , and the cooling flow is turned on. Then an iterative cycle begins. The heaters are turned on for a certain amount of time, Δt_{Hot} , allowing the temperature of the busbar end to reach T_{Hot} . Then the heaters are turned off for a certain amount of time, Δt_{Cold} , allowing the temperature to reach T_{Cold} . If either the number of cycles have reached a certain maximum, N_{max} , or the force is under a certain minimum, F_{min} , the cooling flow is turned off, the test is stopped and the data is analyzed. Otherwise, the process goes through another iterative cycle. Fig. 2 further explains the procedure specification.

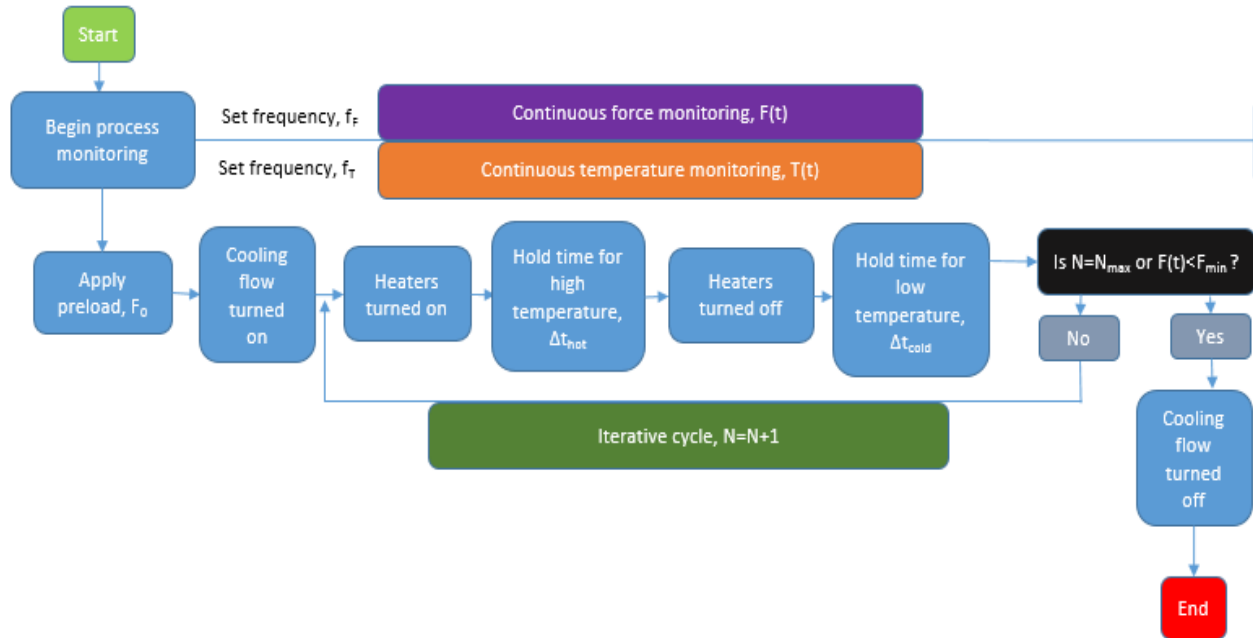


Fig. 2 Designed test protocol for the clamping force relaxation experiment

Two experiments were made for each material using different temperature interval. The first experiment for each material had a peak temperature of around 150 °C while the second one had a peak temperature of around 195 °C. Both of these peak temperatures are the peaks measured by the thermocouple closest to the source of the heat, the cartridge heaters. The lower peak temperature tests were much shorter in timespan than the higher peak temperature ones. The sampling frequencies f_f and f_T were both 1 second. For the lower temperature test, the heating cycle was so that the heaters were on for 30 s and then turned off for 30 s. For the higher temperature test the heating cycle was a little different, the heaters were on for 50 s and off for 20. Both experiments used a preload force of 40 kN. The contact surface area between the washers and the busbar ends was estimated to be 0.00023 m², thus the initial contact pressure is estimated as 170 MPa.

Weld characterization

Bending, tensile and electrical resistance test specimen were extracted from a single 200 mm long, 6 mm thick, optimized AA1050-H14/24 – Cu-OF-04 FSW weld as can be seen from Fig. 3. Similarly, Scanning Electron Microscopy (SEM), Electron Microscopy (EM) and hardness mapping specimens were taken from the middle section of an identical 200 mm long weld.

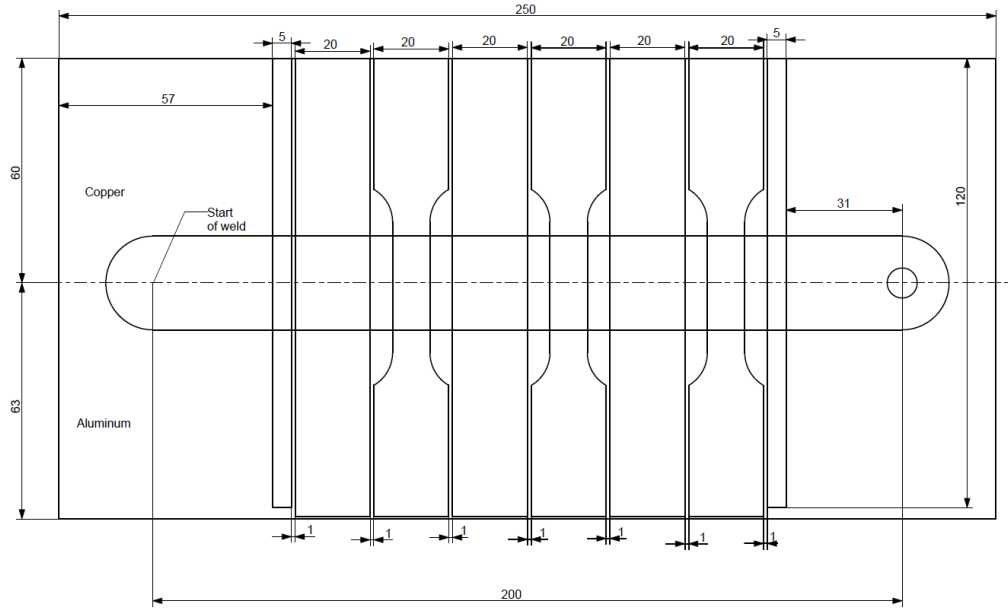


Fig. 3 Specimen extraction plan for mechanical and electrical tests. From right, the first three specimens are for: Electrical test, tensile test, bending test. Dimensions in millimeters.

To assess the performance of the dissimilar Al-Cu FSW joints, three performance parameters were used: Global Efficiency to Tensile Strength (GETS), Global Efficiency to Bending (GEB) for the mechanical properties and the conductivity efficiency (σ_{eff}), for assessment of the electrical resistance. GETS and GEB compare the various bending and tensile properties of the weld to those of the base material [9]. In this work, the mechanical properties of the weld are compared to those of the weaker base material, AA1050-H14/24. An emphasis was put on the ductility of the joints over their strength and so the performance parameters are as follows:

$$GETS = 0.05 \frac{E_i}{E_{BM}} + 0.2 \frac{\sigma_{y-i}}{\sigma_{y_{BM}}} + 0.2 \frac{\sigma_{UTS-i}}{\sigma_{UTS_{BM}}} + 0.25 \frac{A_i}{A_{BM}} + 0.3 \frac{U_{T-i}}{U_{T_{BM}}} \quad (1)$$

$$GEB = 0.4 \frac{F_i}{F_{BM}} + 0.3 \frac{d_i}{d_{BM}} + 0.3 \frac{U_{B-i}}{U_{B_{BM}}} \quad (2)$$

$$\sigma_{eff} = \frac{R_{Al} + R_{Cu}}{R_{Al} + R_{Cu} + R_{Joint}} \quad (3)$$

Where R_{Al} and R_{Cu} are the electrical resistances a 12 mm long segment of each base material with a 5 mm by 6 mm cross-section has.

Bending testing – For the optimized welding condition, two specimens were tested using 3-point bend testing. One test was made for each side, root and face, using a MTS 810 Material Test System at a constant speed of 10 mm/min. The distance between the supporting rollers was 78 mm. To assess the overall bending performance of the weld a performance parameter, Global Efficiency to Bending (GEB),

Tensile testing – Three specimens were tested for the optimized welding condition. The tensile tests were conducted using an MTS 858 Table Top System. A 25 mm extensometer was used for registering the strain rate. Test speed for all tests was 1 mm/min.

Electrical resistance testing – The electrical resistance of the joint was measured and evaluated using a Cropico D07 microhmmeter. Resistance between two points on each side of the weld was measured and then the resistance contribution of the base materials subtracted to acquire the joint’s electrical resistance. See Fig. 4 and equation 1 for further clarification. The cross-section of the electrical resistance samples is 5 mm by 6 mm.

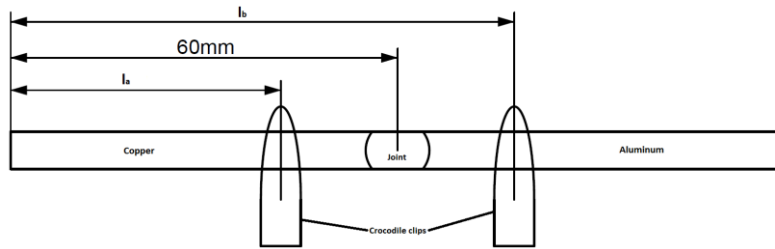


Fig. 4 Schematic of electrical resistance measurements. The copper bar used for the optimized weld had a constant width of 60 mm.

$$R_{Joint} = R_{Measured} - \frac{1000(60 - l_a)\rho_{Cu}}{w_{Cu}h_{Cu}} - \frac{1000(l_b - 60)\rho_{Al}}{w_{Al}h_{Al}} \quad (4)$$

For comparison, the contact resistance between the base materials was measured using varying contact forces. The base materials were cut into samples having the same cross-section as the weld specimens and their ends milled. Then they were clamped together using a small vice and the resistance over the contact measured for low, medium and high forces. The lowest force was so that the samples would stay in place but could easily be moved by hand. Medium force was so that the samples could not be moved by hand and high force was when the vice was tightened as much as possible.

Hardness – Microhardness measurements of a cross-section of the weld were made using a CSM micro-combi tester. 451 indentations were made with an indentation load of 0.5 N. The measurement matrix covered a 20 mm by 5 mm area containing the different weld zones and base materials present in the weld. The Oliver and Pharr measurement method was used to determine the hardness of the indentations.

OM and SEM – Specimens for optical microscopy were polished using diamond paste down to 1 μm. Keller’s solution was used for the etching of the Al side while the Cu was etched using: 100 mL of distilled water, 4mL of saturated sodium chloric, 2 g of potassium dichromate and 5 mL sulphuric acid. Optical micrographs were made with a Nikon Epiphot 200 microscope. SEM was made using a Zeiss Ultra 55 field emission scanning electron microscope. Energy dispersive x-ray spectroscopy (EDX) line analysis was done using the same equipment.

3. Analysis of results

Clamping force relaxation experiment

The clamping force relaxes at a higher rate for EN-EW-6101-T4 than for Cu-OF-04. The difference in force relaxation becomes clearer with higher peak temperature cycles. When T_{max} is $190^{\circ}C$, the Al lowers to 25.2 kN after 881 cycles while the force on the Cu lowers to 32.9 kN after 1236 cycles. When T_{max} is $150^{\circ}C$ the force on the Al lowers to 29.7 kN after 331 cycles while the force on the Cu lowers to 34.2 kN after 358 cycles. Table 1 details the clamping force in the 4 different tests at 300 and 800 cycles as well as the change in force per cycle between 100 and 200 cycles. Fig. 5 displays the force and temperature data collected for the experiment conducted on EN-EW-6101-T4 using $190^{\circ}C$ T_{max} . Fig. 6 explains the positions of the three thermocouples used for temperature data collection in the previously mentioned experiment. Fig. 7 displays the force and temperature data collected for the experiment conducted on Cu-OF-04 using $190^{\circ}C$ T_{max} and Fig. 8 explains the positions of the thermocouples used for temperature data collection.

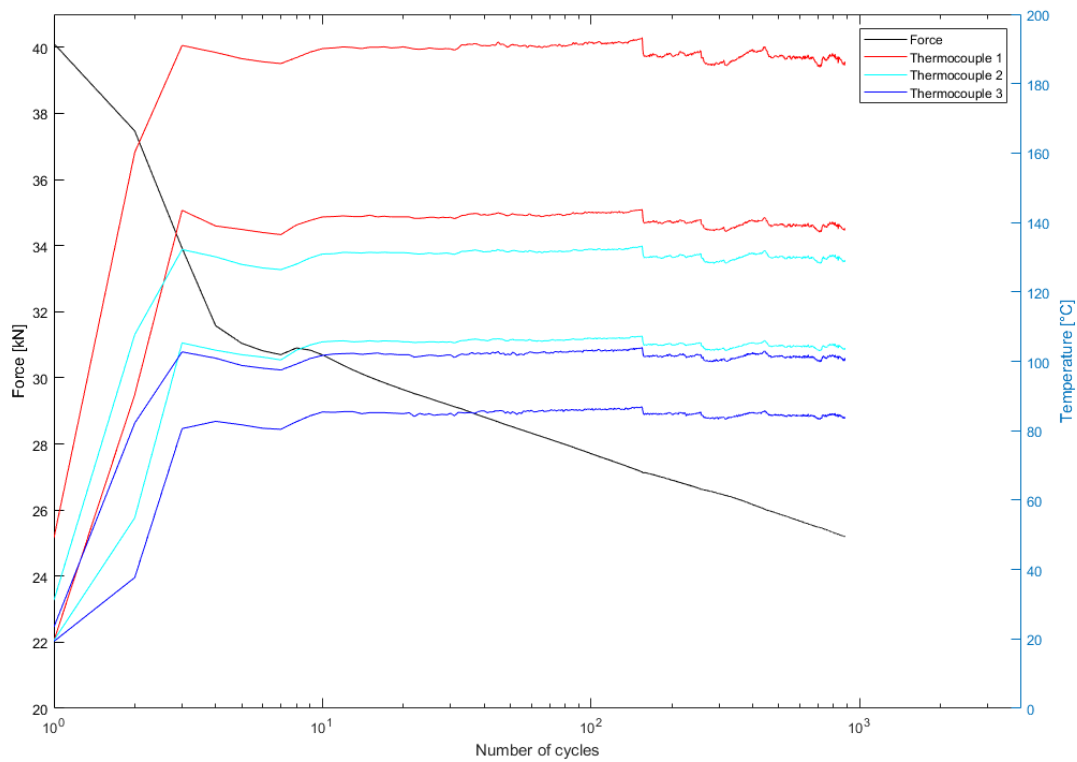


Fig. 5 Force and temperature data for EN-EW-6101-T4 test at $190^{\circ}C$ T_{max} . The force displayed is the average force during each cycle while the temperature curves display the maximum and minimum temperatures recorded by the three different thermocouples each cycle.

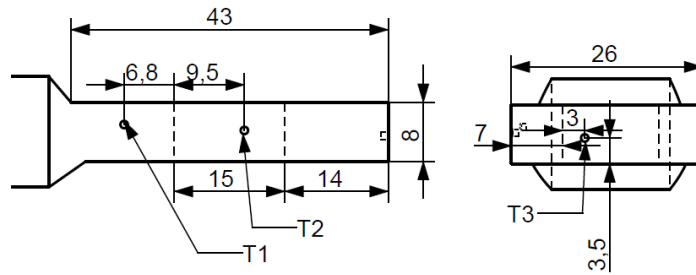


Fig. 6 Thermocouple positions for EN-EW-6101-T4 test at 190° C T_{max} .

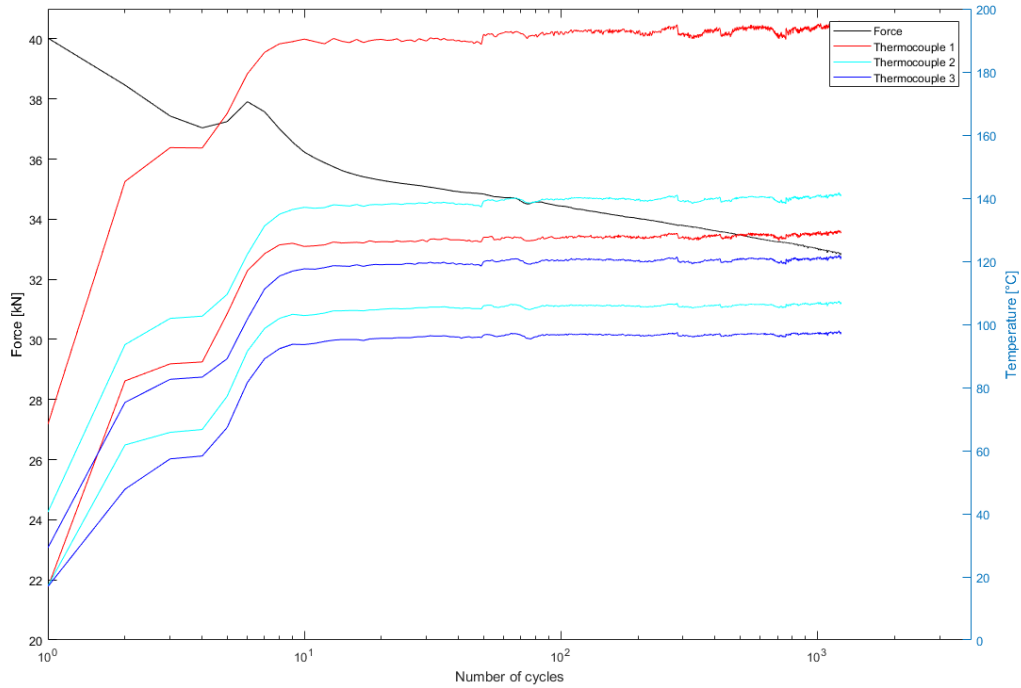


Fig. 7 Force and temperature data for Cu-OF-04 test at 190° C T_{max} . The force displayed is the average force during each cycle while the temperature curves display the maximum and minimum temperatures recorded by the three different thermocouples each cycle.

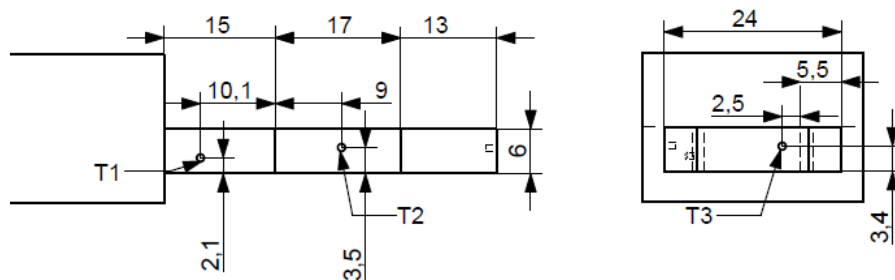


Fig. 8 Thermocouple positions for EN-EW-6101-T4 test at 190° C T_{max} .

Table 1 Main results of the clamping force relaxation experiment detailing the clamping force at different cycles as well as the average change in clamping force between cycles 100-200 for each material.

| T_{max} | Material | $F@300$ cycles | $F@800$ cycles | $\Delta F/cycle@100-200$ cycles |
|-----------|---------------|----------------|----------------|---------------------------------|
| 150 °C | Cu-OF-04 | 34.2 kN | N/A | -3.2 N |
| | EN-EW-6101-T4 | 29.8 kN | N/A | - 9.4 N |
| 190 °C | Cu-OF-04 | 33.8 kN | 33.2 kN | - 4.2 N |
| | EN-EW-6101-T4 | 26.5 kN | 25.3 kN | - 8.1 N |

Tensile, bending and electric resistance results

The results from the tensile tests show GETS as 85%. As seen from Fig. 9, two of the three tensile specimens have high toughness and elongation although a lower ultimate tensile strength than sample 2. These two specimens fractured at the Al side of the weld, where the base material had been thermally affected. Sample 2 fractured in the weld itself. These varying results of the tensile tests is the cause for the relatively high error limits of the results, displayed in Table 2.

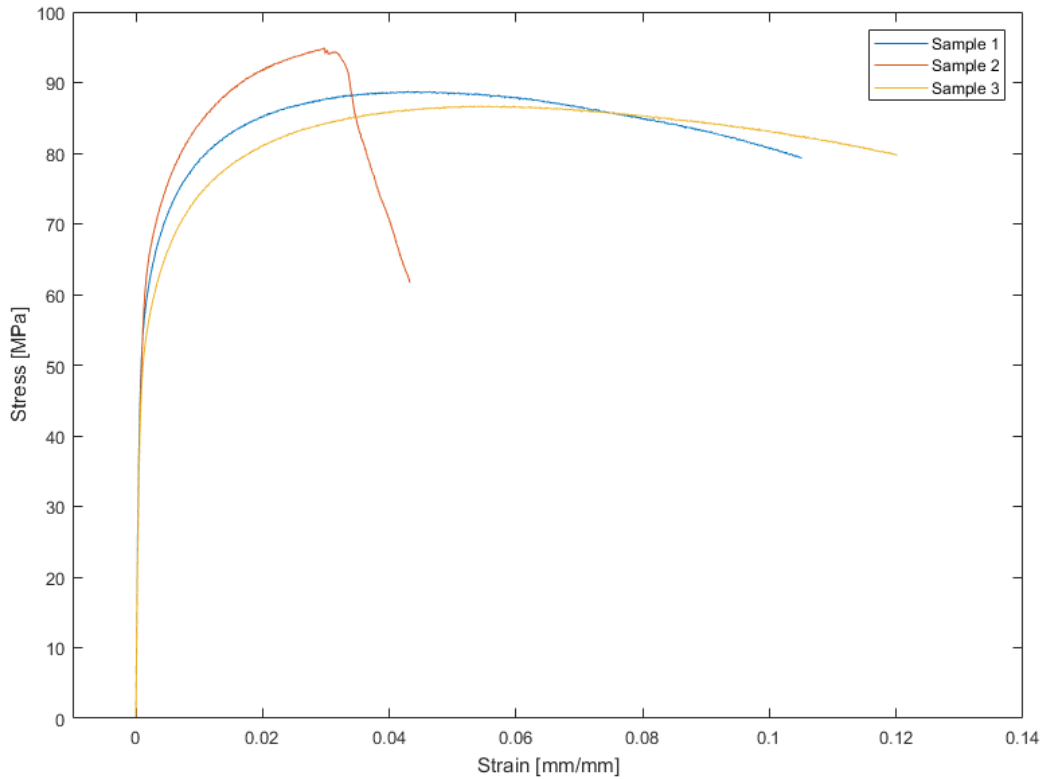


Fig. 9 Engineering stress-strain curves from the tensile tests

Table 2 Tensile properties of the FSW joint

| E [GPa] | σ_y [MPa] | σ_{UTS} [MPa] | A [%] | U_T [J/mm ²] | GETS |
|-----------|------------------|----------------------|-------------|----------------------------|-------------|
| 90.54 ± 2 | 64.09 ± 2.9 | 90.14 ± 4.3 | 26.80 ± 4.8 | 4.32 ± 1.6 | 0.848 ± 0.1 |

There is small difference in the bending properties of the two sides of the joint, the root side being more efficient. The results from the bending tests show GEB as 41%. Fig. 10 displays the bending stress-strain curves from the bending tests made for both directions and the bending properties of the weld can be seen in Table 3.

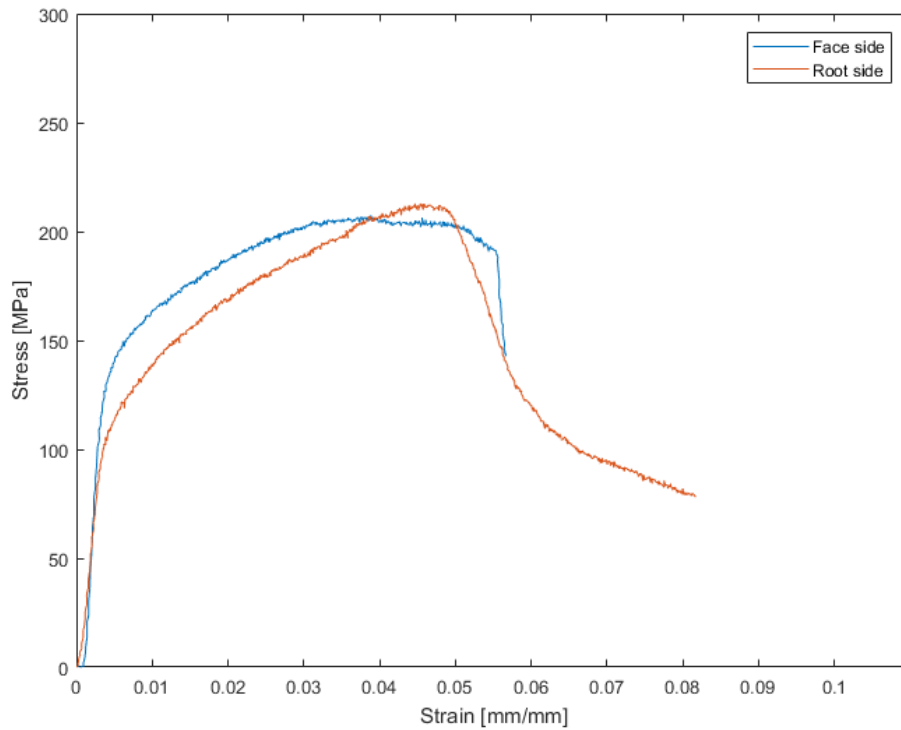


Fig. 10 Bending stress-strain curves from the 3-point bending tests

Table 3 Bending properties of the FSW joint

| Side | F_{max} [kN] | $d@F_{max}$ [mm] | U_B [J/mm ³] | GEB | GEB _{average} |
|------|----------------|------------------|----------------------------|-------|------------------------|
| Face | 1.28 | 6.56 | 6.64 | 0.396 | 0.408 ± 0.02 |
| Root | 1.31 | 7.55 | 7.26 | 0.419 | |

The joint resistance is very small compared to the contact resistance between Al and Cu in clamped joints [10, 11]. This amount of resistance cannot be measured using normal electrical multimeters and is almost negligible as the resistance is only around 3% higher than for a perfect resistless joint. The joint is highly capable of transferring electricity with minimal to negligible power losses. The resistance of the joint is 200 times lower than the contact resistance between the base materials while under a high force. Table 5 displays the contact resistance results.

Table 4 Electrical resistance properties of the FSW joint

| Joint resistance [μΩ] | Proportional increase [%] | σ_{eff} |
|-----------------------|---------------------------|----------------|
| 0,55 ± 1 | 2.9 ± 5 | 0.972 ± 0.05 |

Table 5 Contact resistance between 6 mm by 5 mm surfaces of Cu-OF-04 and AA1050-H14/24 while subjected to various forces

| Force | Contact resistance [$\mu\Omega$] |
|--------|------------------------------------|
| Low | 8000 ± 2000 |
| Medium | 340 ± 30 |
| High | 110 ± 30 |

Hardness test results

Fig. 11 shows the clear difference in the hardness of the base materials, on each side of stirred zone. The Cu has hardness of 120 Vickers while the Al is around 40 Vickers. The stirred zone itself has a more complicated distribution of hardness. Cu tongues and particles, with higher hardness, enter the Al and result in the locally higher hardness fields engulfed by the softer Al. IMCs form at the bottom of the stirred zone and cause the spikes in hardness seen there while the other mixed regions closer to the Cu have hardness values in between that of the base materials.

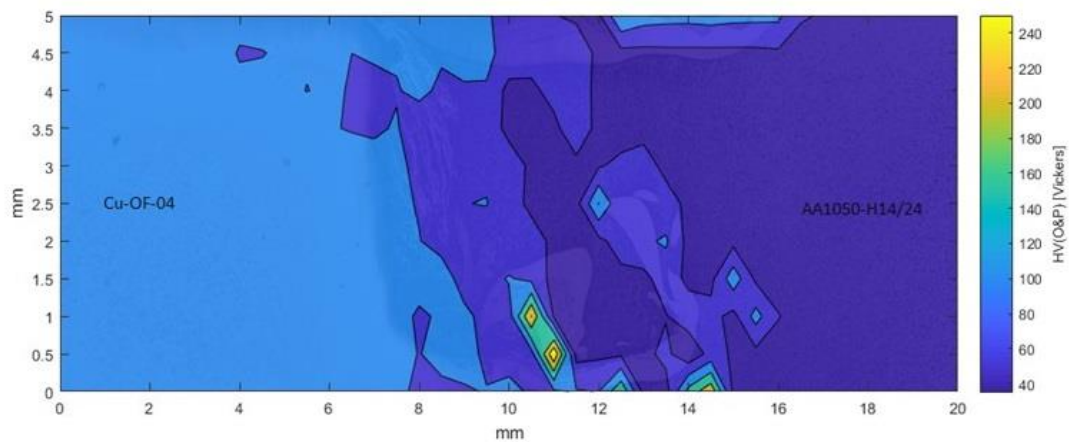


Fig. 11 Microhardness field of the optimized joint, with the optical macrograph transparent in the background

Microstructure analysis

Fig. 12 shows the optical macrograph of the weld and marks the areas of interest that Fig. 13 details further. Figures 14 and 15 display the SEM macrograph of the weld and detailed images of areas of interest.



Fig. 12 Optical macrograph of the optimized weld, areas of interest detailed by Fig. 13 are marked from 1 to 6

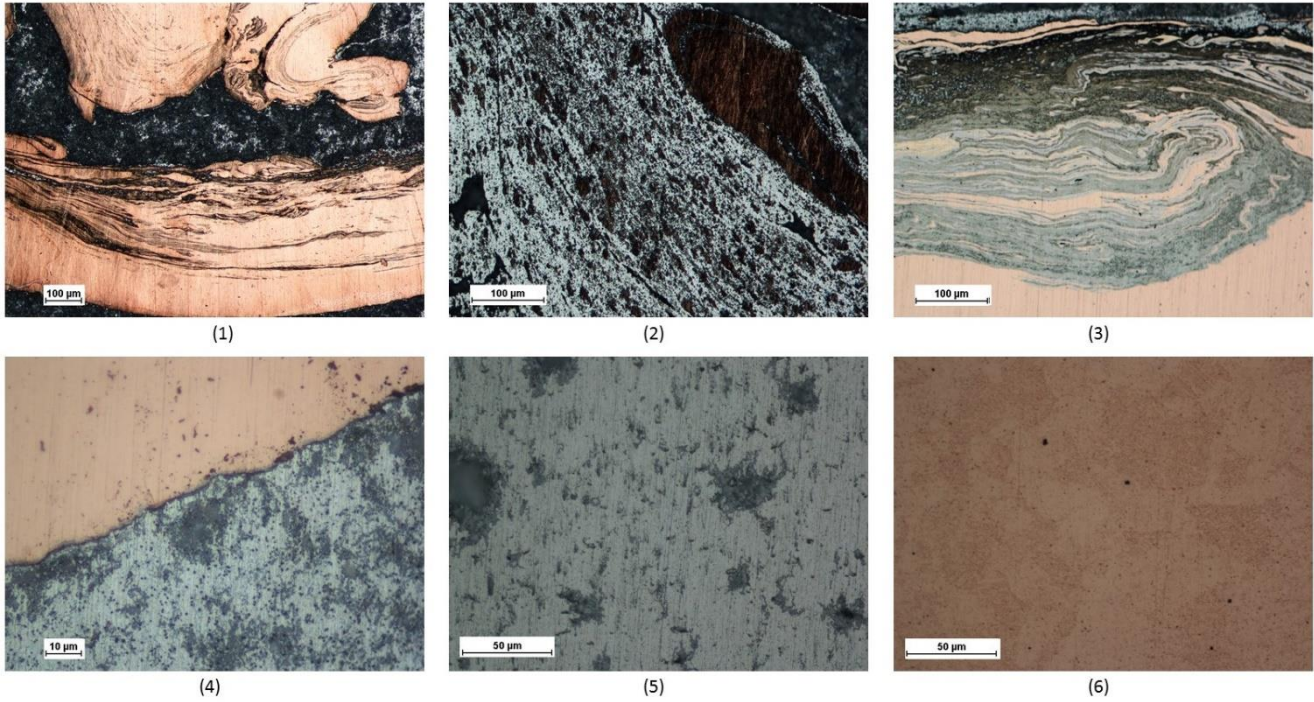


Fig. 13 Micrographs of the joint shown in Fig. 12 from position 1 to 6, (1) Cu-rich mixed material inside the lower Cu tongue, (2) intercalated lamellae, (3) layered structure inside the upper Cu tongue, (4) intermetallic layer, (5) Al grains, (6) Cu grains.

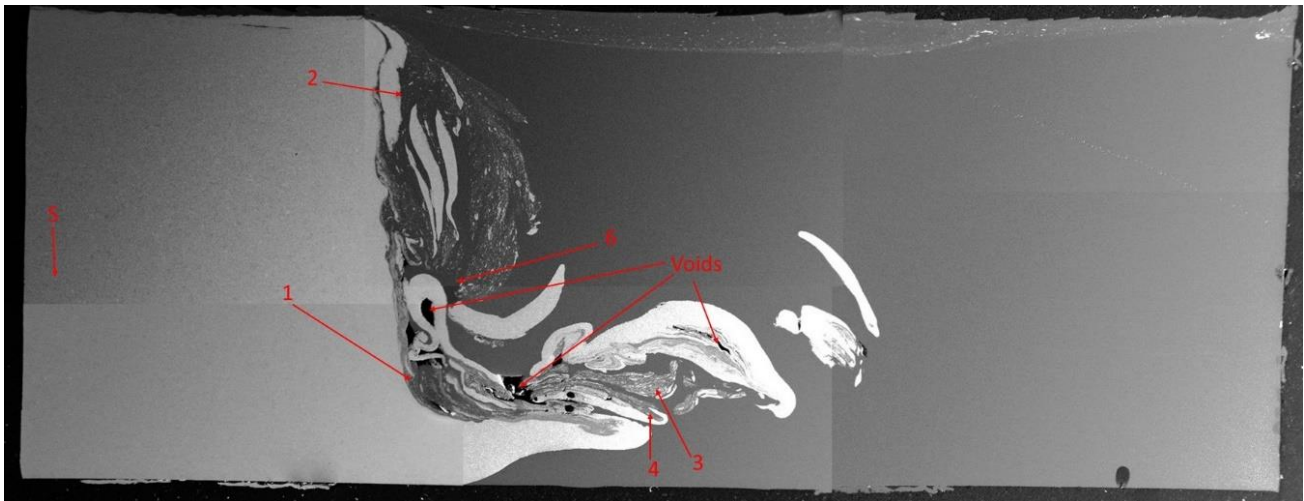


Fig. 14 SEM macrograph of the joint, with areas of interest detailed by Fig. 15 marked from 1-6

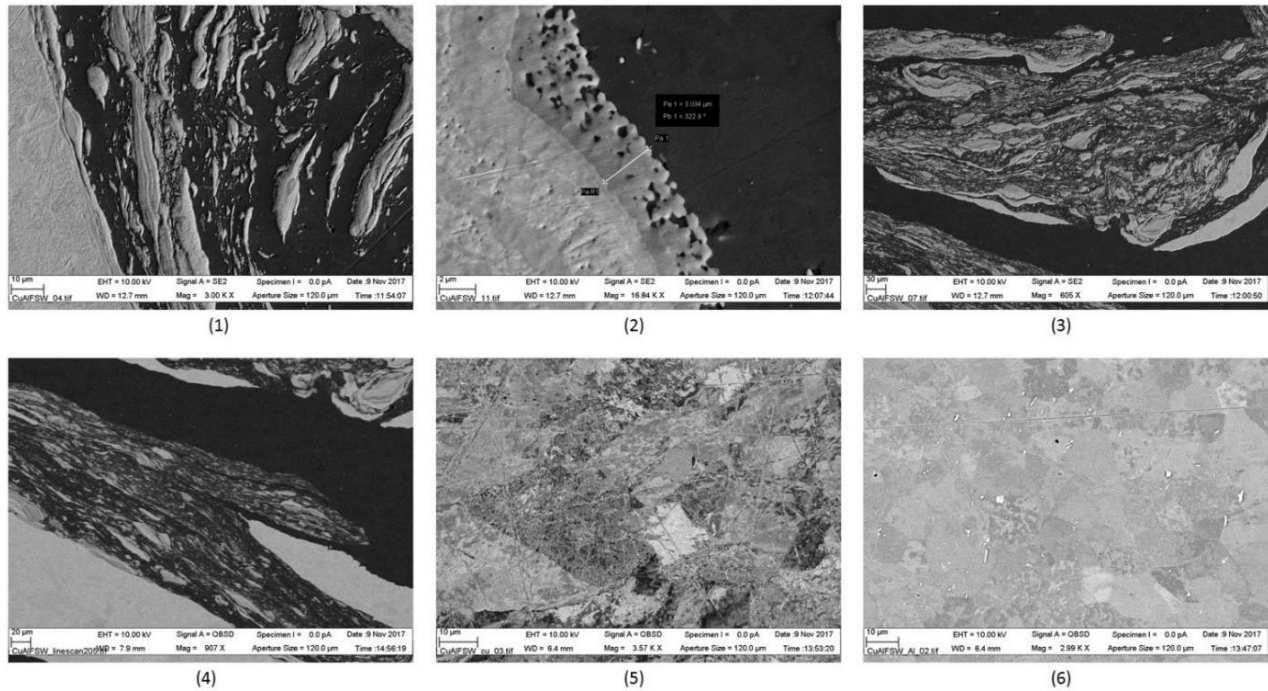


Fig. 15 SEM Micrographs of the joint shown in Fig. 14 from position 1 to 6, (1) Al based composite matrix, (2) IMC layer at the Al-Cu interface, (3) intercalated lamellae, (4) multilayered structure, (5) Cu grains away from the mixed zone, (6) Al grains with Cu particles in the stirred zone.

Figures 12 and 14 show similar weld morphologies, being from the same weld. Different Al-Cu interaction patterns can be identified such as intercalated lamellae in Fig. 13(2) and 15(3). This morphology usually consists of two or more IMC phases and the formation is deeply influenced by process parameters such as rotational speed and tool offset as reported by Galvao *et al.* [8] and Liu *et al.* [12]. Composite-like structures composing of Cu, Cu-rich or IMC particles dispersed in an Al or Al-rich matrix are more easily identified from the SEM imaging, both in the macrograph and more closely in Fig. 15(1). Homogeneous mixtures as characterized by Galvao *et al.* [13] are not found within either sample. A few voids can be seen within the processed zone in Fig. 14. The voids are present in the processed zone on the boundaries between Cu and Al and within Cu dominated mixtures. IMC layers are found in both samples as can be seen from Fig. 13(4) and 15(2). Fig. 16 details the energy dispersive x-ray spectroscopy (EDX) line analysis of the IMC layer found in the SEM sample. The dark gray layer next to the bulk Al was measured having 3 μm thickness and identified as CuAl . Further into the Cu other IMCs such as Cu_9Al_4 are present.

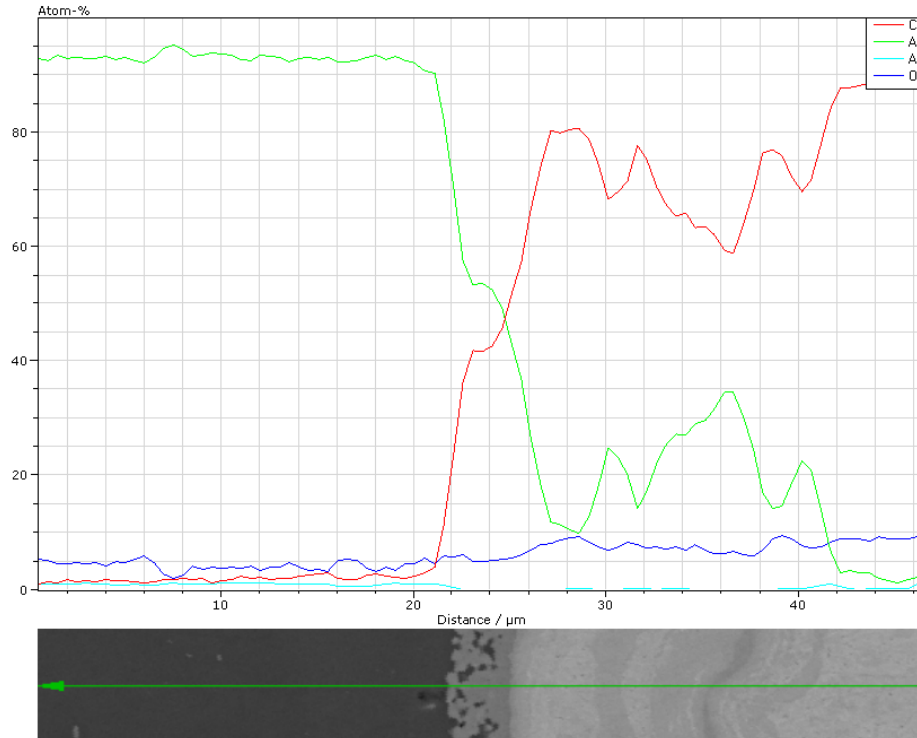


Fig. 16 EDX analysis of the IMC layer seen in Fig. 15 (2)

The line analysis uncovers the IMCs found in the Al-Cu interface. The dark gray layer next to the Al was identified as CuAl. Further into the Cu other more Cu-heavy IMCs are present such as Cu₉Al₄.

4. Conclusions

Difference in clamping force behavior between Cu-OF-04 and EN-EW-6106-T4, an Al alloy used in conventional monolithic Al bus bars, during operational conditions was investigated:

- Cu-OF-04 relaxes at a half a rate compared to the Al alloy and therefore would require much less maintenance. Raising the peak temperatures affecting the materials affects the Al alloy more than the Cu.

A 6 mm AA1050-H14/24 – Cu-OF-04 FSW joint, optimized with busbar production in mind, was characterized for its mechanical, electrical and metallurgical properties.

- The performance parameters for the weld produced with these parameters are as follows:
 - Global Efficiency to Tensile Strength (GETS), compared to Al: 0.85
 - Global Efficiency to Bending (GEB), compared to Al: 0.41
 - Electrical Conductive Efficiency, compared to an ideal resistless joint: 0.97
- Metallurgical investigation of the optimized joints shows an intense mixture of materials with large amounts of multilayered structures, both Al-matrix composite and intercalated lamellae. Occasional voids were observed.
- Intermetallic compounds were found in the weld, both emerging as particles in various mixtures as well as layers. The largest single compound layer identified was measured to be around 3 μm.

- FSW joints produced have negligible electrical resistance compared to the resistance between clamped base materials (200 times lower resistance).

References

- [1] W. S. Loewenthal and D. L. Ellis, "Fabrication of GRCop-84 Rocket Thrust Chambers," 2005.
- [2] J. R. Davis and J. R. Davis, *Aluminum and Aluminum Alloys*. ASM international, 1993.
- [3] F. Nix and D. MacNair, "The thermal expansion of pure metals: copper, gold, aluminum, nickel, and iron," *Physical Review*, vol. 60, (8), pp. 597, 1941.
- [4] W. Thomas, "Friction stir butt welding," *International Patent Application no.PCT/GB92/0220*, 1991.
- [5] D. Lohwasser and Z. Chen, *Friction Stir Welding: From Basics to Applications*. Elsevier, 2009.
- [6] T. DebRoy and H. Bhadeshia, "Friction stir welding of dissimilar alloys—a perspective," *Science and Technology of Welding and Joining*, vol. 15, (4), pp. 266-270, 2010.
- [7] G. E. Schulze, *Metallphysik: Ein Lehrbuch*. Springer-Verlag, 2013.
- [8] I. Galvao, J. Oliveira, A. Loureiro and D. Rodrigues, "Formation and distribution of brittle structures in friction stir welding of aluminium and copper: influence of process parameters," *Science and Technology of Welding and Joining*, vol. 16, (8), pp. 681-689, 2011.
- [9] P. Vilaça and W. Thomas, "Friction stir welding technology," in *Structural Connections for Lightweight Metallic Structures* Anonymous Springer, 2011, pp. 85-124.
- [10] W. Bonwitt, "An Experimental Investigation of the Electrical Performance of Bolted Aluminium-to-Copper Connections," *Transactions of the American Institute of Electrical Engineers*, vol. 67, (2), pp. 1208-1219, 1948.
- [11] R. Jackson, "Electrical performance of aluminium/copper bolted joints," in *IEE Proceedings C (Generation, Transmission and Distribution)*, 1982, pp. 177-184.
- [12] H. J. Liu, J. J. Shen, S. Xie, Y. X. Huang, F. Cui, C. Liu and L. Y. Kuang, "Weld appearance and microstructural characteristics of friction stir butt barrier welded joints of aluminium alloy to copper," *Science and Technology of Welding and Joining*, vol. 17, (2), pp. 104-110, 02/01, 2012.
- [13] I. Galvão, A. Loureiro and D. M. Rodrigues, "Critical review on friction stir welding of aluminium to copper," *Science and Technology of Welding and Joining*, vol. 21, (7), pp. 523-546, 10/02, 2016.